GEOPHYSICS, VOL. 77, NO. 2 (MARCH-APRIL 2012); P. C27–C35, 8 FIGS.
10.1190/GEO2011-0228.1

Numerical test of the Schoenberg-Muir theory

José M. Carcione[1], Stefano Picotti[1], Fabio Cavallini[1], and Juan E. Santos[2]

ABSTRACT

The Schoenberg-Muir theory states that an equivalent, homogeneous and anisotropic medium can be constructed from a layered medium composed of several thin layers, each anisotropic, under the assumption of stationarity. To test the theory we considered single transversely isotropic layers with different orientations of the symmetry axis and performed numerical simulations of wave propagation with a full-wave solver. The equivalent media have orthorhombic and monoclinic symmetries, respectively. The theory performed very well from the kinematical and dynamical points of view, even for strong anisotropy and layers described by media whose symmetry axes have different orientations.

INTRODUCTION

The field of effective anisotropy as industrial practice has increased substantially during the last twenty years due to improvements in seismic acquisition (multicomponent data and azimuthal coverage), the advent of more accurate prestack depth migration methods, a wider range of source-receiver offsets, and the development of practical parameter-estimation algorithms. The subject of effective media theories for fractured reservoirs is important in exploration seismology because it may reveal information about permeability anisotropy and therefore, about the preferred direction of the fluid flow (Grechka and Kachanov, 2006a, b). The complexity of the reservoir structure (layering and fracture orientations) requires the use of realistic rheologies, so the future trend is to go beyond transverse isotropy and employ lower-symmetry models, such as orthorhombic and monoclinic (Tsvankin et al., 2010).

Thin transversely isotropic layers with a vertical symmetry axis (VTI media) behave as a homogeneous, transversely isotropic medium when the wavelength is much longer than the thicknesses. To our knowledge, the first to study the problem using VTI layers was Bruggeman (1937). Other investigators analyzed the problem using different approaches, e.g., Riznichenko (1949) and Postma (1955), who considered a two-constituent periodically layered medium. Later, Backus (1962) showed that periodicity is not necessary and also obtained the effective elasticity constants with a strict formulation of averages by integrals. He assumed stationarity, i.e., in a given length of composite medium much smaller than the wavelength, the proportion of each material is constant (see Helbig, 1963).

Schoenberg and Muir (1989) extended Backus' approach to single layers of arbitrary anisotropy using group theory and a matrix formalism. However, this generalization has been questioned by Hudson and Crampin (1991), who argue that the theory cannot be applied to oblique sets of cracks (even for weak anisotropy), because the structure is no longer 1D, and Backus' assumptions are invalidated (see response in Schoenberg and Muir, 1991). More recently, Helbig (1999) solved the problem of Schoenberg and Muir (1989) without recourse to group theory, but he did not discuss its validity.

Backus averaging has been verified numerically by Carcione et al. (1991), who found that the minimum ratio between the P-wave dominant pulse wavelength and the spatial period of the layering depends on the contrast between the constituents. For instance, for a periodic sequence of epoxy-glass it is around eight, and for sandstone-limestone (which has a lower reflection coefficient) it is between five and six. In any case, a minimum ratio can be found above which the equivalence between a finely layered medium and a homogeneous, transversely isotropic medium is valid.

The purpose of this paper is to verify, by way of numerical example, the Schoenberg-Muir theory against the criticism of Hudson and Crampin (1991). We consider a periodic sequence of VTI-ψTI layers, where ψTI is the VTI medium rotated by an angle ψ about the y-axis. In particular, we consider $\psi = \pi/2$ and $\pi/4$. The resulting equivalent media have orthorhombic and monoclinic symmetries, respectively. We compute the wavefield

Manuscript received by the Editor 27 June 2011; revised manuscript received 14 October 2011; published online 6 March 2012.
[1]Istituto Nazionale di Oceanografia e di Geofisica Sperimentale (OGS), Trieste, Italy. E-mail: jcarcione@inogs.it; spicotti@inogs.it; fcavallini@inogs.it.
[2]CONICET, Universidad de Buenos Aires, Facultad de Ingeniería, Instituto de Gas y del Petróleo, Buenos Aires, Argentina; Universidad Nacional de La Plata, La Plata, Argentina; and Purdue University, Department of Mathematics, W. Lafayette, Indiana, USA. E-mail: santos@math.purdue.edu.

with a modeling method used by Carcione et al. (1991), generalized to the anisotropic case. Details of this space-time-domain direct method can be found in Carcione et al. (1988).

SCHOENBERG-MUIR THEORY

Let us consider a finely layered medium composed of N arbitrarily anisotropic layers (Figure 1), with the z-axis perpendicular to the layering plane. Each layer is defined by the density ρ, the proportion p_n, and the elastic constants c_{IJ}. The stress-strain relation of each layer can be written as

$$\begin{pmatrix}\sigma_1\\ \sigma_2\\ \sigma_6\\ \\ \sigma_3\\ \sigma_4\\ \sigma_5\end{pmatrix}=\begin{pmatrix}\sigma_{11}\\ \sigma_{22}\\ \sigma_{12}\\ \\ \sigma_{33}\\ \sigma_{23}\\ \sigma_{13}\end{pmatrix}=\begin{pmatrix}c_{11} & c_{12} & c_{16} & c_{13} & c_{14} & c_{15}\\ c_{12} & c_{22} & c_{26} & c_{23} & c_{24} & c_{25}\\ c_{16} & c_{26} & c_{66} & c_{36} & c_{46} & c_{56}\\ & & & & & \\ c_{13} & c_{23} & c_{36} & c_{33} & c_{34} & c_{35}\\ c_{14} & c_{24} & c_{46} & c_{34} & c_{44} & c_{45}\\ c_{15} & c_{25} & c_{56} & c_{35} & c_{45} & c_{55}\end{pmatrix}\begin{pmatrix}e_1\\ e_2\\ e_6\\ \\ e_3\\ e_4\\ e_5\end{pmatrix}, \tag{1}$$

where σ_I denotes stress component and e_I denotes strain component in the Voigt notation (e.g., Carcione, 2007). The stiffness matrix involved in equation 1 can be rewritten in terms of four submatrices as

$$\begin{pmatrix}C_{TT} & C_{TN}\\ C_{TN}^{\mathsf{T}} & C_{NN}\end{pmatrix}. \tag{2}$$

According to Schoenberg and Muir (1989), the equivalent homogeneous medium is defined by the following matrix:

$$\begin{pmatrix}\bar{C}_{TT} & \bar{C}_{TN}\\ \bar{C}_{TN}^{\mathsf{T}} & \bar{C}_{NN}\end{pmatrix}, \tag{3}$$

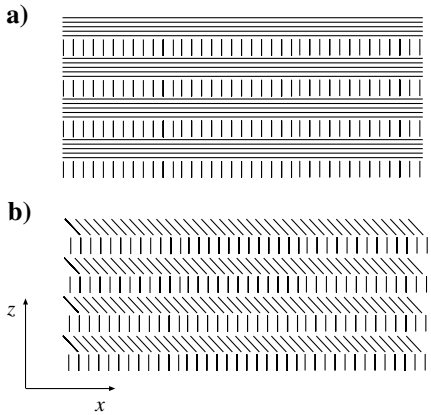

Figure 1. Stack of thin (compared to the wavelength) strata composed of HTI and VTI layers (a) and 45TI and VTI layers (b). The percentage of each constituent is assumed to be stationary with respect to the vertical coordinate.

where

$$\begin{aligned}\bar{C}_{NN} &= \langle C_{NN}^{-1}\rangle^{-1},\\ \bar{C}_{TN} &= \langle C_{TN}C_{NN}^{-1}\rangle\bar{C}_{NN},\\ \bar{C}_{TT} &= \langle C_{TT}\rangle - \langle C_{TN}C_{NN}^{-1}C_{NT}\rangle + \bar{C}_{TN}\langle C_{NN}^{-1}C_{NT}\rangle,\end{aligned} \tag{4}$$

where the thickness weighted average of a quantity C is defined as

$$\langle C\rangle = \sum_{n=1}^{N} p_n C_n. \tag{5}$$

In this work, we consider periodic systems of equal composition whose single layers have transversely isotropic symmetry (VTI) or rotated versions of this medium, ψTI, where ψ is the rotation angle of the symmetry axis from the vertical. Specifically, we consider VTI = 0TI, HTI = 90TI, and 45TI media as shown in Figure 1. The new elasticity matrix after rotation of a medium is given in Appendix A.

The equivalent elasticity matrices for VTI-HTI and VTI-45TI periodic systems are given in Appendix B, where $p_1 = p_2 = 1/2$ and HTI and 45TI indicate the same VTI medium whose symmetry axis is rotated by the angles $\psi = \pi/2$ and $\psi = \pi/4$, respectively.

TIME-DOMAIN MODELING IN MONOCLINIC MEDIA

We consider the symmetry plane of a monoclinic medium, say, the (x, z)-plane, and recast the equation of motion in the particle-velocity/stress formulation (Carcione, 2007). In this plane, we identify two sets of uncoupled differential equations:

$$\begin{aligned}\dot{v}_1 &= \rho^{-1}(\partial_1\sigma_{11} + \partial_3\sigma_{13} + f_1),\\ \dot{v}_3 &= \rho^{-1}(\partial_1\sigma_{13} + \partial_3\sigma_{33} + f_3),\\ \dot{\sigma}_{11} &= c_{11}\partial_1 v_1 + c_{13}\partial_3 v_3 + c_{15}(\partial_1 v_3 + \partial_3 v_1),\\ \dot{\sigma}_{33} &= c_{13}\partial_1 v_1 + c_{33}\partial_3 v_3 + c_{35}(\partial_1 v_3 + \partial_3 v_1),\\ \dot{\sigma}_{13} &= c_{15}\partial_1 v_1 + c_{35}\partial_3 v_3 + c_{55}(\partial_1 v_3 + \partial_3 v_1),\end{aligned} \tag{6}$$

and

$$\begin{aligned}\dot{v}_2 &= \rho^{-1}(\partial_1\sigma_{12} + \partial_3\sigma_{23} + f_2),\\ \dot{\sigma}_{23} &= c_{44}\partial_3 v_2 + c_{46}\partial_1 v_2,\\ \dot{\sigma}_{12} &= c_{46}\partial_3 v_2 + c_{66}\partial_1 v_2,\end{aligned} \tag{7}$$

where v_i are the particle-velocity components, ρ is the density, f_i are external forces, a dot above a variable denotes time differentiation and ∂_i indicates the spatial partial derivative with respect to the variable x_i. The strain vector and the particle-velocity components are related as

$$\begin{pmatrix} \dot{e}_1 \\ \dot{e}_2 \\ \dot{e}_3 \\ \dot{e}_4 \\ \dot{e}_5 \\ \dot{e}_6 \end{pmatrix} = \begin{pmatrix} \partial_1 v_1 \\ \partial_2 v_2 \\ \partial_3 v_3 \\ \partial_2 v_3 + \partial_3 v_2 \\ \partial_1 v_3 + \partial_3 v_1 \\ \partial_1 v_2 + \partial_2 v_1 \end{pmatrix}. \tag{8}$$

The first set of equations 6 describes in-plane particle motion while the second set 7 describes cross-plane particle motion, that is, the propagation of a pure shear wave. The uncoupling implies that a cross-plane shear wave exists at a plane of mirror symmetry. The plane-wave analysis, including the calculation of the phase and group velocities, is given in Appendix C.

The numerical algorithm used to solve the equation of motion is based on the Fourier pseudospectral method for computing the spatial derivatives and a fourth-order Runge-Kutta technique for calculating the wavefield recursively in time (e.g., Carcione, 2007).

SIMULATIONS

We consider the qP-qS case and

$$\begin{pmatrix} c_{11} & c_{13} & c_{15} \\ c_{13} & c_{33} & c_{35} \\ c_{15} & c_{35} & c_{55} \end{pmatrix} = \begin{pmatrix} 46 & 18 & 0 \\ 18 & 30 & 0 \\ 0 & 0 & 7 \end{pmatrix}, \tag{9}$$

in GPa. In this case, c_{12} needs not to be specified because it has no influence on the results. The velocity-anisotropy coefficient for P-waves is defined as the fractional difference between the horizontal and vertical velocities:

$$A = 100\frac{\sqrt{c_{11}} - \sqrt{c_{33}}}{\sqrt{c_{33}}}.$$

Its value is $A = 24\%$ for the elasticity matrix defined in equation 9. According to equations B-1 and B-5, rotations of $\pi/2$ and $\pi/4$ yield

$$\begin{pmatrix} 30 & 18 & 0 \\ 18 & 46 & 0 \\ 0 & 0 & 7 \end{pmatrix} \quad \text{and} \quad \begin{pmatrix} 35 & 21 & -4 \\ 21 & 35 & -4 \\ -4 & -4 & 10 \end{pmatrix}, \tag{10}$$

respectively. From equations B-4 and B-6, the effective VTI-HTI and VTI-45TI media have the following elasticity matrices:

$$\begin{pmatrix} 38 & 18 & 0 \\ 18 & 36.3 & 0 \\ 0 & 0 & 7 \end{pmatrix} \quad \text{and} \quad \begin{pmatrix} 40 & 19 & -1.6 \\ 19 & 31.9 & -1.5 \\ -1.6 & -1.5 & 8.1 \end{pmatrix}, \tag{11}$$

respectively. We take $\rho = 2600$ kg/m^3. Figure 2 shows the group (energy) velocity curves corresponding to the orthorhombic (Figure 2a) and monoclinic (Figure 2b) effective media. The VTI medium is rotated to obtain the HTI (45TI) medium and then the VTI and HTI (45TI) are averaged to obtain the effective orthorhombic (VTI-HTI) and monoclinic (VTI-45TI) media.

The source used in the simulations is a vertical force (f_1) with the following time history:

$$h(t) = \left(u - \frac{1}{2}\right)\exp(-u), \qquad u = \left[\frac{\pi(t - t_s)}{t_p}\right]^2, \tag{12}$$

where t_p is the period of the wave, $f_p = 1/t_p$ is the central frequency and we take $t_s = 1.4t_p$.

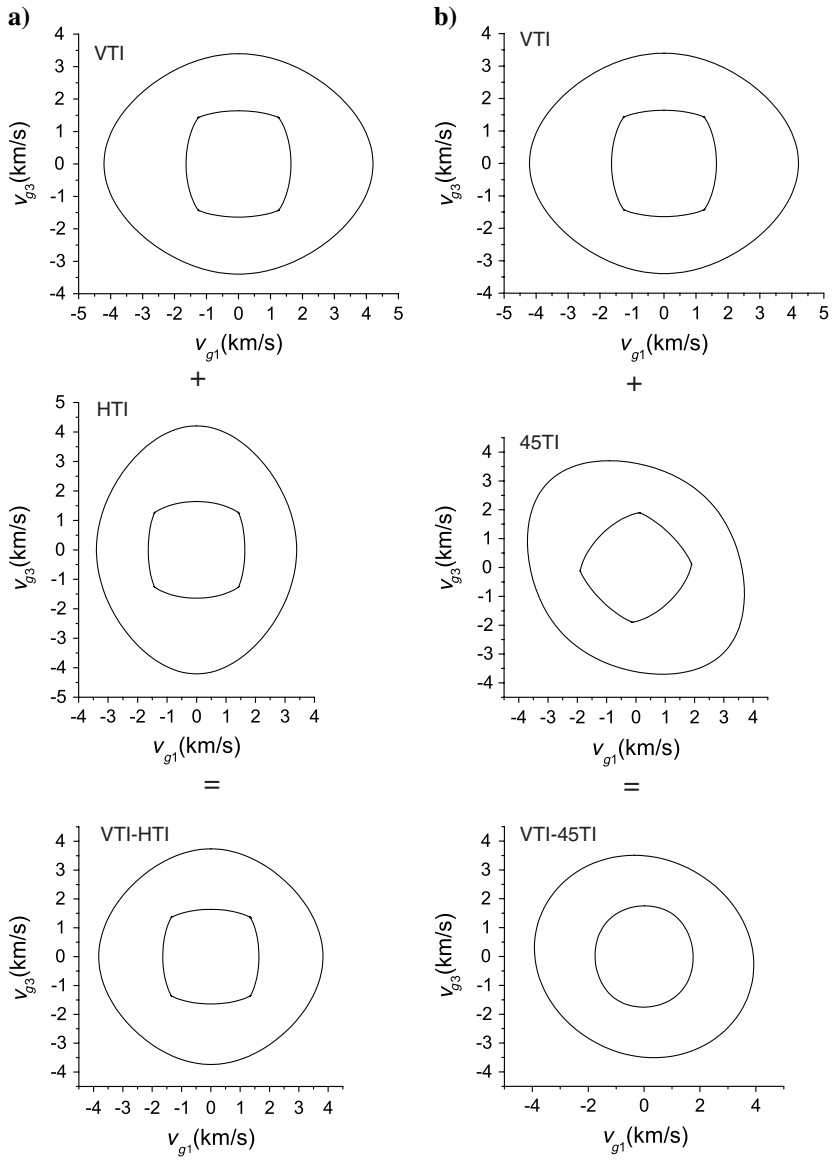

Figure 2. Group (energy) velocity curves corresponding to the orthorhombic (a) and monoclinic (b) effective media. The VTI medium is rotated to obtain the HTI (45TI) medium and then the VTI and HTI (45TI) are averaged to obtain the effective orthorhombic VTI-HTI (monoclinic VTI-45TI) medium.

The simulations use a 455×455 mesh with 1-m grid spacing and the central frequency of the source is $f_p = 80$ Hz. The force is located at the center of the mesh. The Runge-Kutta algorithm has a time step of 0.1 ms and snapshots of the vertical particle-velocity v_3 are computed at 70 ms. The snapshots corresponding to the group-velocity curves shown in Figure 2 are displayed in Figure 3, where it is verified that the modeling code reproduces correctly the predictions of the plane-wave analysis.

The wavelength/thickness ratio can be defined as

$$R = \sqrt{\frac{c}{\rho}} \frac{1}{f_p P}, \tag{13}$$

where c is c_{11} for P-waves and c_{55} for S (the maximum velocity has been considered, see equation 9) and P is the period of the stratification, in this case, $P = 2$ m, i.e., each layer has 1-m thickness. In this specific simulation, $R = 26$ for P-waves and $R = 10$ for S-waves.

Figure 4 shows the snapshots in the orthorhombic (Figure 4a) and monoclinic (Figure 4b) effective (Schoenberg-Muir) media (upper pictures). The lower pictures display the simulations in the finely layered media. As can be seen, the snapshots are indistinguishable, indicating that the Schoenberg-Muir theory provides a good approximation to fine layering at long wavelengths.

To better appreciate the similarity of the results, Figure 5 shows the seismogram at $(x, z) = (57, 57)$ m from the source location for

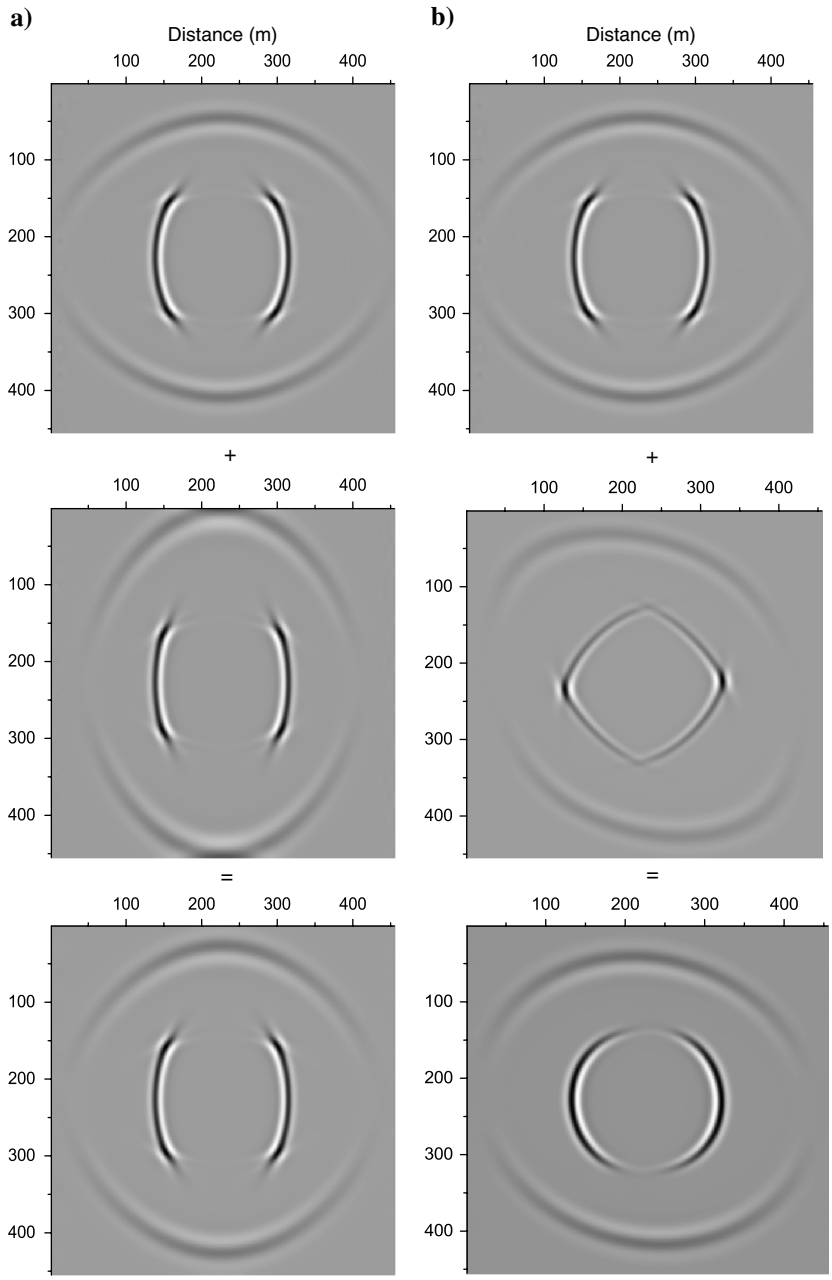

Figure 3. Snapshots corresponding to the group-velocity curves shown in Figure 2. The lower ones refer to the equivalent (Schoenberg-Muir) media.

the VTI-HTI orthorhombic (Figure 5a) and VTI-45TI monoclinic (Figure 5b) media. The solid line corresponds to the effective (Schoenberg-Muir) monoclinic medium and the dots to the simulations in the finely layered medium. As can be seen, the agreement is excellent.

We have also considered a VTI medium defined by

$$\begin{pmatrix} c_{11} & c_{13} & c_{15} \\ c_{13} & c_{33} & c_{35} \\ c_{15} & c_{35} & c_{55} \end{pmatrix} = \begin{pmatrix} 60 & 3 & 0 \\ 3 & 30 & 0 \\ 0 & 0 & 7 \end{pmatrix}, \qquad (14)$$

which has an anisotropy coefficient $A = 41\%$ (see group-velocity in Figure 6) and obtained an excellent match between the results of the theory and the simulations in layered media. This can be appreciated in Figure 7, where a snapshot (Figure 7a) and the seismogram (Figure 7b) at $(x, z) = (52, 52)$ m from the source location for the VTI-45TI monoclinic medium are shown. In this case, the source central frequency is $f_p = 50$ Hz and its highest significant frequency component is approximately 100 Hz.

Finally, we perform a simulation with a receiver outside the symmetry planes. In this case, we use a 3D modeling code based on the Fourier pseudospectral method (Helbig and Carcione, 2009). We do not implement any absorbing boundary at the sides of the grid, so that the medium is periodic. This means that a wave impinging on the left boundary of the grid will return from the right boundary.

We consider the VTI-HTI composite medium, with

$$c_{11} = 46, c_{12} = 12, c_{13} = 18, c_{33} = 30, c_{55} = 7 \quad \text{and}$$
$$c_{66} = 17 (\text{VTI medium}),$$
$$c_{11} = 30, c_{12} = c_{13} = 18, c_{23} = 12,$$
$$c_{22} = c_{33} = 46, c_{44} = 17, \quad \text{and}$$
$$c_{55} = c_{66} = 7 (\text{HTI medium})$$

(in GPa). The velocity-anisotropy coefficient for SH waves in VTI media, defined as $100(\sqrt{c_{66}} - \sqrt{c_{55}})/\sqrt{c_{66}}$, is 36%. The effective medium is orthorhombic with the stiffness coefficients

$$c_{11} = 38, c_{12} = 15, c_{13} = 18, c_{22} = 45.8,$$
$$c_{23} = 15.6, c_{33} = 36.3, c_{44} = 9.9, c_{55} = 7, \quad \text{and}$$
$$c_{66} = 12 (\text{in GPa}).$$

The simulations use a 81^3 mesh with a cell size of 1 m and the central frequency of the source is $f_p = 80$ Hz. A vertical force is located at the center of the mesh and the seismogram (z-component, see Figure 8) is computed at $(x, y, z) = (10, 10, 10)$ m from the source location. The solid line corresponds to the effective medium and the dots to the simulations in the finely layered medium. The agreement is as good as in the symmetry planes.

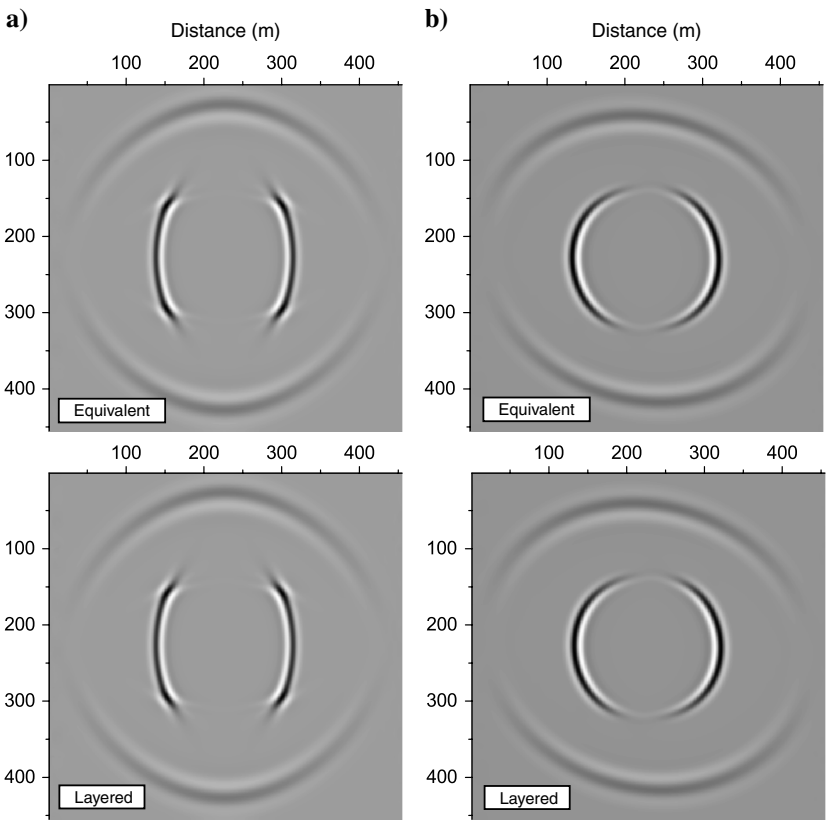

Figure 4. Snapshots in the orthorhombic (a) and monoclinic (b) effective (Schoenberg-Muir) media (upper panels). The lower panels display the simulations in the finely layered media. The outer and inner wavefronts correspond to the qP- and qS-waves, respectively.

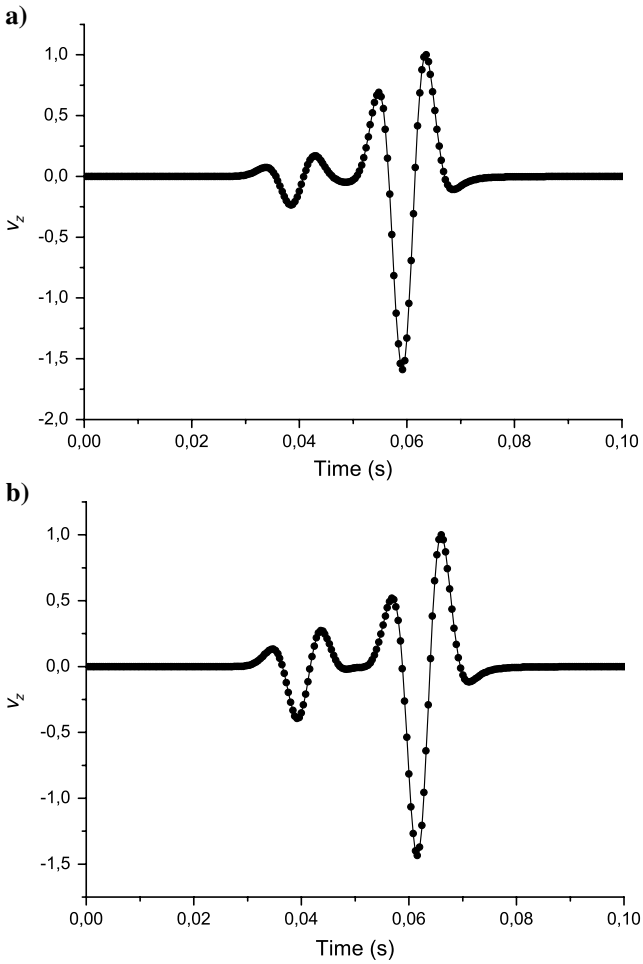

Figure 5. Seismogram at $(x, z) = (57, 57)$ m from the source location. The solid line corresponds to the effective (Schoenberg-Muir) medium and the dots to the simulations in the finely layered medium. (a) Orthorhombic medium; (b) monoclinic medium. The VTI thin layer has 24% anisotropy.

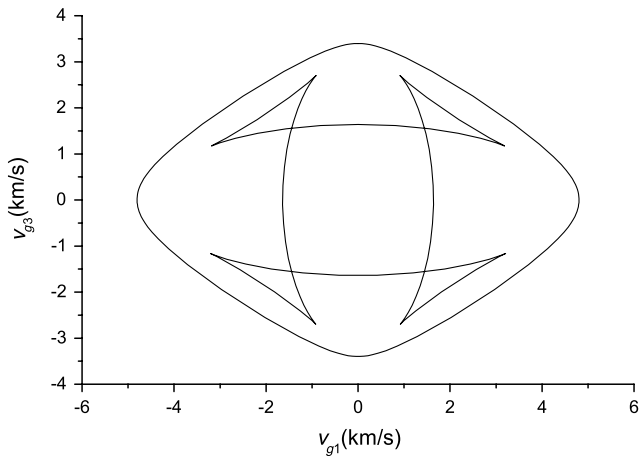

Figure 6. Group-velocity curve corresponding to a strongly anisotropic VTI medium. The VTI thin layer has 41% anisotropy. This medium and its rotated version (45TI) are used to obtain the effective VTI-45TI medium.

These simulations show that the theory performs very well, no matter the degree of anisotropy. The only limitation is that the layers have to be very thin compared to the minimum wavelength of the signal; to be rigorous, the theory is exact at zero frequency. The theory performs equally well for amplitudes, going beyond the expectations of the authors because they state (Schoenberg and Muir, 1989), "The real limitation is the long-wavelength one, which says, in effect, that it is concerned with kinematics arrival times-alone. It does not address the important dynamical question of how high-frequency energy is lost from the coherent to the scattered field." It is evident in Figures 5, 7, and 8 that at long wavelengths, the theory performs equally well for amplitudes.

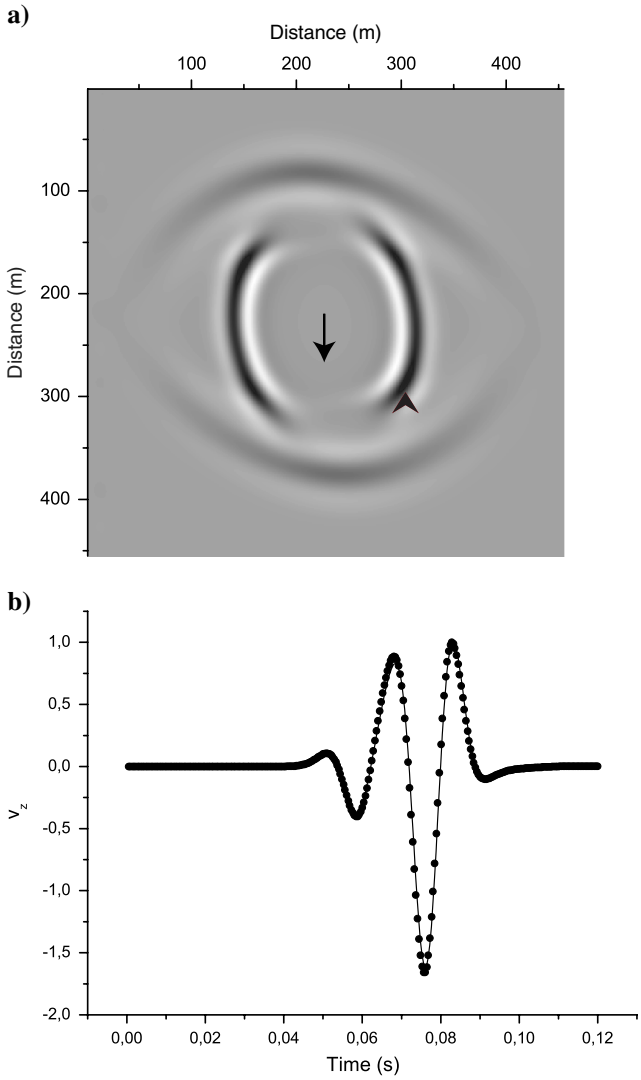

Figure 7. Snapshot in the effective monoclinic medium at 70 ms (a) and seismogram at $(x, z) = (52, 52)$ m from the source location (b). The solid line corresponds to the effective (Schoenberg-Muir) monoclinic medium (VTI-45TI) and the dots to the simulations in the finely layered medium. The VTI thin layer has 41% anisotropy (see Figure 6). The arrow and the triangle indicate the source and receiver, respectively.

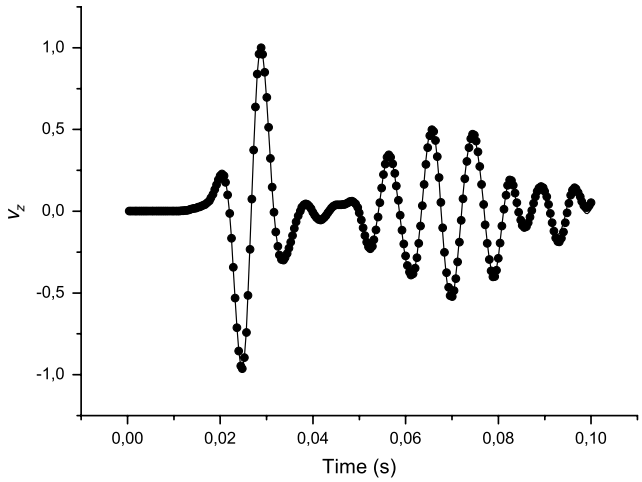

Figure 8. Seismogram at $(x, y, z) = (10, 10, 10)$ m (outside the symmetry planes) from the source location. The solid line corresponds to the effective orthorhombic medium and the dots to the simulations in the finely layered medium.

CONCLUSIONS

We performed numerical simulations (snapshots and time histories) of wave propagation in a layered medium whose layers are anisotropic and thin compared to the wavelength, and compared the results to similar simulations in an equivalent medium obtained from the Schoenberg-Muir theory. The assumptions of the theory (Backus's assumptions) state that the model works for layer thicknesses small compared to the wavelength, small crack aspect ratios, and very long flat parallel fractures and fracture spacings. Under these conditions, the Schoenberg-Muir theory is valid from the kinematic (traveltimes) and dynamic (amplitudes) points of view, no matter how anisotropic are the single constituent layers. Even for constituent transversely isotropic layers with tilted axis (e.g., obliquely aligned cracks [the monoclinic case]), the theory performs equally well. The theory is not limited to cracks and fractures, but the anisotropy of the single layers can be due to other causes, such as fine layering.

ACKNOWLEDGMENTS

This paper is dedicated to the memory of Michael A. Schoenberg. We thank Klaus Helbig for useful comments.

APPENDIX A

ELASTICITY MATRIX OF A ROTATED MEDIUM

A VTI medium with symmetry axis along the z-axis has the following stiffness matrix

$$\mathbf{C} = \begin{pmatrix} c_{11} & c_{12} & c_{13} & 0 & 0 & 0 \\ c_{12} & c_{11} & c_{13} & 0 & 0 & 0 \\ c_{13} & c_{13} & c_{33} & 0 & 0 & 0 \\ 0 & 0 & 0 & c_{55} & 0 & 0 \\ 0 & 0 & 0 & 0 & c_{55} & 0 \\ 0 & 0 & 0 & 0 & 0 & c_{66} \end{pmatrix}, \qquad \text{(A-1)}$$

$$2c_{66} = c_{11} - c_{12}.$$

A clockwise rotation of the vertical symmetry axis through an angle ψ about the y-axis has the orthogonal transformation matrix:

$$\begin{pmatrix} \cos\psi & 0 & \sin\psi \\ 0 & 1 & 0 \\ -\sin\psi & 0 & \cos\psi \end{pmatrix}. \qquad \text{(A-2)}$$

The corresponding Bond transformation matrix is (Carcione, 2007)

$$\mathbf{M} = \begin{pmatrix} \cos^2\psi & 0 & \sin^2\psi & 0 & \sin(2\psi) & 0 \\ 0 & 1 & 0 & 0 & 0 & 0 \\ \sin^2\psi & 0 & \cos^2\psi & 0 & -\sin(2\psi) & 0 \\ 0 & 0 & 0 & \cos\psi & 0 & -\sin\psi \\ -\frac{1}{2}\sin(2\psi) & 0 & \frac{1}{2}\sin(2\psi) & 0 & \cos(2\psi) & 0 \\ 0 & 0 & 0 & 0 & 0 & \cos\psi \end{pmatrix}. \qquad \text{(A-3)}$$

Then, the stiffness matrix with the rotated symmetry axis is given by (Carcione, 2007),

$$\mathbf{C}' = \mathbf{M} \cdot \mathbf{C} \cdot \mathbf{M}^{\top}. \qquad \text{(A-4)}$$

APPENDIX B

EFFECTIVE ELASTICITY MATRIX FOR VTI-HTI AND VTI-45TI MEDIA

First, we consider a periodic system of VTI and HTI layers, where the HTI medium, labeled 2, is the same VTI medium, labeled 1. Using A-4, an angle $\psi = \pi/2$ transforms a VTI medium into an HTI medium,

$$\begin{pmatrix} c_{11} & c_{12} & c_{13} & 0 & 0 & 0 \\ c_{12} & c_{11} & c_{13} & 0 & 0 & 0 \\ c_{13} & c_{13} & c_{33} & 0 & 0 & 0 \\ 0 & 0 & 0 & c_{55} & 0 & 0 \\ 0 & 0 & 0 & 0 & c_{55} & 0 \\ 0 & 0 & 0 & 0 & 0 & c_{66} \end{pmatrix}$$

$$\rightarrow \begin{pmatrix} c_{33} & c_{13} & c_{13} & 0 & 0 & 0 \\ c_{13} & c_{11} & c_{12} & 0 & 0 & 0 \\ c_{13} & c_{12} & c_{11} & 0 & 0 & 0 \\ 0 & 0 & 0 & c_{66} & 0 & 0 \\ 0 & 0 & 0 & 0 & c_{55} & 0 \\ 0 & 0 & 0 & 0 & 0 & c_{55} \end{pmatrix}. \qquad \text{(B-1)}$$

According to equations 1, 3, and B-1,

$$C_{TT}^{(1)}=\begin{pmatrix} c_{11} & c_{12} & 0\\ c_{12} & c_{11} & 0\\ 0 & 0 & c_{66}\end{pmatrix},\quad C_{TN}^{(1)}=\begin{pmatrix} c_{13} & 0 & 0\\ c_{13} & 0 & 0\\ 0 & 0 & 0\end{pmatrix},$$
$$C_{NN}^{(1)}=\begin{pmatrix} c_{33} & 0 & 0\\ 0 & c_{55} & 0\\ 0 & 0 & c_{55}\end{pmatrix}, \tag{B-2}$$

and

$$C_{TT}^{(2)}=\begin{pmatrix} c_{33} & c_{13} & 0\\ c_{13} & c_{11} & 0\\ 0 & 0 & c_{55}\end{pmatrix},\quad C_{TN}^{(2)}=\begin{pmatrix} c_{13} & 0 & 0\\ c_{12} & 0 & 0\\ 0 & 0 & 0\end{pmatrix},$$
$$C_{NN}^{(2)}=\begin{pmatrix} c_{11} & 0 & 0\\ 0 & c_{66} & 0\\ 0 & 0 & c_{55}\end{pmatrix}, \tag{B-3}$$

with $c_{66}=\frac{1}{2}(c_{11}-c_{12})$.

Using equation 3, the effective medium composed of VTI-HTI layers has orthorhombic symmetry and is given by the following symmetric elasticity matrix

$$\begin{pmatrix} \frac{c_{11}+c_{33}}{2} & \frac{c_{12}+c_{13}}{2} & c_{13} & 0 & 0 & 0\\ * & c_{11}-\frac{(c_{12}-c_{13})^2}{2(c_{11}+c_{33})} & \frac{c_{11}c_{13}+c_{12}c_{33}}{c_{11}+c_{33}} & 0 & 0 & 0\\ * & * & \frac{2c_{11}c_{33}}{c_{11}+c_{33}} & 0 & 0 & 0\\ * & * & * & \frac{2(c_{11}-c_{12})c_{55}}{c_{11}-c_{12}+2c_{55}} & 0 & 0\\ * & * & * & * & c_{55} & 0\\ * & * & * & * & * & \frac{1}{4}(c_{11}-c_{12}+2c_{55}) \end{pmatrix}. \tag{B-4}$$

Now, we consider a periodic system of VTI and 45TI layers, where the 45TI medium, labeled 2, is the same VTI medium, but rotated by 45°. An angle $\psi=\pi/4$ transforms a VTI medium into an 45TI medium, whose (symmetric) elasticity matrix is

$$\begin{pmatrix} a+c_{55} & \frac{1}{2}(c_{12}+c_{13}) & a-c_{55} & 0 & \frac{1}{4}(c_{33}-c_{11}) & 0\\ * & c_{11} & \frac{1}{2}(c_{12}+c_{13}) & 0 & \frac{1}{2}(c_{13}-c_{12}) & 0\\ * & * & a+c_{55} & 0 & \frac{1}{4}(c_{33}-c_{11}) & 0\\ * & * & * & b & 0 & \frac{1}{4}(-c_{11}+c_{12}+2c_{55})\\ * & * & * & * & \frac{1}{4}(c_{11}-2c_{13}+c_{33}) & 0\\ * & * & * & * & * & b \end{pmatrix}, \tag{B-5}$$

with

$$4a=c_{11}+2c_{13}+c_{33},\quad 4b=c_{11}-c_{12}+2c_{55}.$$

Combining the 45TI and VTI media, the effective medium has monoclinic symmetry and is given by the following symmetric elasticity matrix

$$\begin{pmatrix} \bar{c}_{11} & \bar{c}_{12} & \bar{c}_{13} & 0 & \bar{c}_{15} & 0\\ * & \bar{c}_{22} & \bar{c}_{23} & 0 & \bar{c}_{25} & 0\\ * & * & \bar{c}_{33} & 0 & \bar{c}_{35} & 0\\ * & * & * & \bar{c}_{44} & 0 & \bar{c}_{46}\\ * & * & * & * & \bar{c}_{55} & 0\\ * & * & * & * & * & \bar{c}_{66} \end{pmatrix}, \tag{B-6}$$

where

$$\begin{aligned}
D\bar{c}_{11} &= c_{11}^2(c_{33}+c_{55})+c_{11}C\\
&\quad +c_{33}[-c_{13}^2+c_{55}(c_{33}+4c_{55})],\\
D\bar{c}_{12} &= c_{13}[c_{33}(-c_{13}+c_{55})+c_{11}(c_{33}+c_{55})]\\
&\quad +c_{12}[C+c_{33}(c_{11}-c_{13})+c_{55}(c_{11}-c_{33})],\\
-D\bar{c}_{13} &= (c_{13}+c_{33})(c_{13}^2-c_{11}c_{33})+2c_{55}[-c_{13}(c_{11}+3c_{33})\\
&\quad +2c_{55}(c_{33}-c_{13})],\\
D\bar{c}_{15} &= c_{55}(-c_{11}+c_{33})(c_{13}+c_{33}+2c_{55}),\\
\bar{c}_{22} &= c_{11}-(c_{12}-c_{13})^2(c_{33}+c_{55})D^{-1},\\
\bar{c}_{23} &= c_{13}-c_{33}(c_{12}-c_{13})(c_{13}-c_{33}-2c_{55})D^{-1},\\
-D\bar{c}_{25} &= c_{55}(c_{12}-c_{13})(c_{13}+3c_{33}+2c_{55}),\\
D\bar{c}_{33} &= 2c_{33}[-c_{13}^2+(c_{11}+2c_{55})(c_{33}+2c_{55})],\\
D\bar{c}_{35} &= 2c_{33}c_{55}(-c_{11}+c_{33}),\\
F\bar{c}_{44} &= 2c_{55}(c_{11}-c_{12}+2c_{55}),\\
D\bar{c}_{46} &= c_{55}(-c_{11}+c_{12}+2c_{55}),\\
D\bar{c}_{55} &= 2c_{55}[-c_{13}^2+(c_{33}+c_{55})(c_{33}-2c_{13})\\
&\quad +c_{11}(2c_{33}+c_{55})],\\
4F\bar{c}_{66} &= (c_{11}-c_{12})^2+4c_{55}[3(c_{11}-c_{12})+c_{55}],\\
C &= -c_{13}^2+c_{33}^2+6c_{33}c_{55}+4c_{55}^2,\\
D &= C-2c_{13}c_{33}+2c_{11}(c_{33}+c_{55}),\\
F &= c_{11}-c_{12}+6c_{55}.
\end{aligned} \tag{B-7}$$

APPENDIX C

PHASE AND GROUP VELOCITIES OF THE EFFECTIVE ANISOTROPIC MEDIUM

In the symmetry plane of a monoclinic medium there is a pure shear wave and two coupled waves. The respective phase velocity surfaces in the (x,z)-plane are

$$\Gamma_{22}-\rho v_p^2=0,\quad (\Gamma_{11}-\rho v_p^2)(\Gamma_{33}-\rho v_p^2)-\Gamma_{13}^2=0, \tag{C-1}$$

where

$$\begin{aligned}
\Gamma_{11} &= c_{11}l_1^2+c_{55}l_3^2+2c_{15}l_1l_3,\\
\Gamma_{22} &= c_{66}l_1^2+c_{44}l_3^2+2c_{46}l_1l_3,\\
\Gamma_{33} &= c_{33}l_3^2+c_{55}l_1^2+2c_{35}l_1l_3,\\
\Gamma_{13} &= c_{15}l_1^2+c_{35}l_3^2+(c_{13}+c_{55})l_1l_3
\end{aligned} \tag{C-2}$$

(Carcione, 2007), where v_p is the phase velocity and $l_1=\sin\theta$ and $l_3=\cos\theta$, with θ the phase propagation angle. The SH-wave group-velocity is

$$\mathbf{v}_g = \frac{1}{\rho v_p}[(c_{66}l_1 + c_{46}l_3)\hat{\mathbf{e}}_1 + (c_{44}l_3 + c_{46}l_1)\hat{\mathbf{e}}_3]. \quad \text{(C-3)}$$

On the other hand, the qP and qS group-velocity components are

$$v_{g1} = \left(\frac{1}{v_p}\right)\frac{(\Gamma_{33} - \rho v_p^2)(c_{11}l_1 + c_{15}l_3) + (\Gamma_{11} - \rho v_p^2)(c_{55}l_1 + c_{35}l_3) - \Gamma_{13}[2c_{15}l_1 + (c_{13} + c_{55})l_3]}{\rho(\Gamma_{11} + \Gamma_{33} - 2\rho v_p^2)} \quad \text{(C-4)}$$

and

$$v_{g3} = \left(\frac{1}{v_p}\right)\frac{(\Gamma_{33} - \rho v_p^2)(c_{55}l_3 + c_{15}l_1) + (\Gamma_{11} - \rho v_p^2)(c_{33}l_3 + c_{35}l_1) - \Gamma_{13}[2c_{35}l_3 + (c_{13} + c_{55})l_1]}{\rho(\Gamma_{11} + \Gamma_{33} - 2\rho v_p^2)}. \quad \text{(C-5)}$$

REFERENCES

Backus, G. E., 1962, Long-wave elastic anisotropy produced by horizontal layering: Journal of Geophysical Research, **67**, 4427–4440, doi: 10.1029/JZ067i011p04427.

Bruggeman, D. A. G., 1937, Berechnungen der verschiedener physikalischen konstanten von heterogenen substanzen. III: Die elastischen konstanten der quasi-isotropen mischkörper aus isotropen substanzen: Annalen der Physik, **421**, 160–178, doi: 10.1002/(ISSN)1521-3889.

Carcione, J. M., 2007, Wave fields in real media: Wave propagation in anisotropic, anelastic, porous and electromagnetic media; Handbook of geophysical exploration, **38**: Elsevier.

Carcione, J. M., D. Kosloff, and A. Behle, 1991, Long wave anisotropy in stratified media: A numerical test: Geophysics, **56**, 245–254, doi: 10.1190/1.1443037.

Carcione, J. M., D. Kosloff, and R. Kosloff, 1988, Wave propagation simulation in an anisotropic (transversely isotropic) medium: Quarterly Journal of Mechanics and Applied Mathematics, **41**, 319–345, doi: 10.1093/qjmam/41.3.319.

Grechka, V., and M. Kachanov, 2006a, Seismic characterization of multiple fracture sets: Does orthotropy suffice?: Geophysics, **71**, no 3, D93–D105, doi: 10.1190/1.2196872.

Grechka, V., and M. Kachanov, 2006b, Effective elasticity of rocks with closely spaced and intersecting cracks: Geophysics, **71**, no. 3, D85–D91, doi: 10.1190/1.2197489.

Helbig, K., 1963, Remarks on paper by G. E. Backus, Long-wave elastic anisotropy produced by horizontal layering: Journal of Geophysical Research, **68**, 3742–3742, doi: 10.1029/JZ068i012p03742.

Helbig, K., 1999, Layer-induced elastic anisotropy — Part 1: Forward relations between constituent parameters and compound medium parameters: Revista Brasileira de Geofísica, **16**, 103–112.

Helbig, K., and J. M. Carcione, 2009, Anomalous polarization in anisotropic media: European Journal of Mechanics, A/Solids, **28**, 704–711.

Hudson, J. A., and S. Crampin, 1991, Discussion on: "A calculus for finely layered anisotropic media," M. Schoenberg, and F. Muir, authors: Geophysics, **56**, 572–575.

Postma, G. W., 1955, Wave propagation in a stratified medium: Geophysics, **20**, 780–806, doi: 10.1190/1.1438187.

Riznichenko, Y. V., 1949, Seismic quasi-anisotropy: Bulletin of the Academy of Sciences of the USSR, Geographical and Geophysical Service, **13**, 518–544.

Schoenberg, M., and F. Muir, 1989, A calculus for finely layered media: Geophysics, **54**, 581–589, doi: 10.1190/1.1442685.

Schoenberg, M., and F. Muir, 1991, Reply by authors to J. A. Hudson, and S. Crampin: Geophysics, **56**, 575–576, doi: 10.1190/1.1486691.

Tsvankin, I., J. Gaiser, V. Grechka, M. van der Baan, and L. Thomsen, 2010, Seismic anisotropy in exploration and reservoir characterization: An overview: Geophysics, **75**, no. 5, A15–A29, doi: 10.1190/1.3481775.